Diagonal bracing of steel frames with multi-cable arrangements

Metin Husem[*1], Serhat Demir[1], Hong G. Park[2] and Suleyman I. Cosgun[1]

[1]*Department of Civil Engineering, Karadeniz Technical University, 61080, Trabzon, Turkey*
[2]*Department of Architecture, Seoul National University, Seoul 151-742, South Korea*

Abstract.   A large number of structure in the world were build with poor seismic details, with or without any lateral load resisting system like concentrically braced frames and steel plate shear walls. These structures can reveal deteriorating hysteretic behaviors with stiffness and strength degradation. Therefore, seismic retrofitting of such structures for drift control has vital importance. In this study a retrofit methodology has been developed, which involves diagonal bracing of steel frames with different cable arrangements. In the experimental and numerical program 5 different lateral load resisting system were tested and results compared with each other. The results indicated that multi-cable arrangements suggested in this study showed stable ductile behavior without any sudden decrease in strength. Due to the usage of more than one diagonal cable, fracture of any cable did not significantly affect the overall strength and deformation capacity of the system. In cable braced systems damages concentrated in the boundary zones of the cables and beams. That is why boundary zone must have enough stiffness and strength to resist tension field action of cables.

Keywords: cable; steel wire rope; concentrically braced frame; steel plate shear wall; FEA

1. Introduction

Inelastic behavior in steel buildings is often a direct result of the lateral translation caused by earthquakes. This can result in severe damage to the building or even total collapse. Although many engineers and researchers develop design codes while keeping the reality of earthquakes and consequent damage in mind, current codes can always be improved upon (Gupta and Krawinkler 1999).

Currently there are several methods that are employed to limit lateral translation in steel structures. Concentrically braced frames (CBFs) are one of the most common lateral load resisting systems for steel buildings. The advantages of CBFs over moment resisting frames (MRFs) for earthquake resistance is seen as better at control of lateral displacement and greater overall strength in the buildings (Tremblay and Filiatrault 1996), The braces, however, can fail through acceptable ductility after several cycles of inelastic deformation, including stretching in tension and buckling in compression (Broderick *et al*. 2008), After compression buckling of steel braces has occurred, the braces are susceptible to fracture at the midspan when they are stretched again in

---

∗Corresponding author, Professor, E-mail: mhusem@ktu.edu.tr

tension. The buckling of braces often decreases their ductility and energy-dissipating capacity under cyclic loading (Tremblay 2001), Premature yielding, buckling, and low-cycle fatigue induced ruptures of braces may be concentrated over several stories in a multi-story steel CBFs that are affected by earthquake loading, triggering a detrimental soft-story failure mechanism (Aguero *et al*. 2006),

Another lateral force resisting system used in steel structures are steel plate shear walls (SPSWs). The main advantages of a SPSW system are the significant additional strength and rigidity compared to other lateral force resisting systems. In the first applications of SPSWs, plate buckling was prevented through the use of a stiffened plate or by selecting an appropriately thick plate. However, Thornburn *et al*. (1983) showed that SPSWs with unstiffened thin plates had both high ductility and high strength even after the local buckling of a thin infill plate. Consequently, SPSWs have advantages over the conventional RC wall in several ways. SPSWs are lighter than RC shear walls, applicable for new design or retrofit projects, and relatively easy to construct (Sabelli and Bruneau 2007), In addition, SPSWs can be economically attractive compared to RC shear walls (Timler *et al*. 1998),

In addition to these, to prevent lateral translation, tension only concentrically braced frames (TOCBFs) and cables (steel wire ropes-SWRs) are also used in regions with low level of seismicity. TOCBFs utilize very slender bracing members, such as steel rods or flat plates, which are unable to dissipate much energy in compression (AISC 2005). The critical disadvantages in the use of these systems are their tendency to buckle easily and become extremely deformed. The main concern of current design codes stems from presence of very large pinching in hysteretic behavior (Tremblay and Filiatrault 1996), Recently Wang *et al*. (2013) have experimentally tested the behavior of two full scale TOCBFs. Obtained results showed that, pinched behavior was occured due to cyclic compression buckling of the braces. To solve pinching problem, Tamai and Takamatsu (2005) proposed a non-compression rod bracing with a special washer/wedge connection. In their proposed connection, the wedge slides between the beveled washer and this would prevent rod buckling. As a result, they eliminated the pinching effect and energy dissipation capability of the rod brace was significantly improved.

Hou and Tagawa (2009) used SWRs with central cylinder for seismic retrofit of moment frames. They concluded that this retrofitting method can increase the lateral stiffness without reducing the moment frame ductility. Fanaie *et al*. (2016) made theoretical studies on cable bracing system with central cylinder. They recommended that dimensions of cylinder should be selected in such a way that the cables also reach their yielding limit. Hadi and Alrudaini (2012) used vertical cables to provide alternate load path to redistribute residual loads and prevent potential progressive collapse of RC buildings. Mouseavi *et al*. (2015), Mouseavi and Zahrai (2016) proposed a slack free connection (SFC) to removed pinching from hysteretic behavior of cable braces. Results indicated that energy dissipation capacity of cable braces with SFC would be improved up to 6 times compared with that of conventional cable braces.

In this paper, the behavior of steel frames which is strengthened with diagonally braced multi-cables were examined. Results obtained from the numerical study were additionally verified through earlier experimental results. Also, the effects of multi-cables were compared with MRFs, CBFs and SPSWs.

2. Numerical study

2.1 Specimens design

In order to be able to check the accuracy of results obtained from the numerical studies, in finite element models (FEMs) respectively named MRF, CBF and SPSW, the size and material properties according to the experimental specimens of Choi and Park (2008), are preferred (Table 1 and Fig. 1), The configurations of finite element models formed to investigate the effects of SWRs are presented in Table 2 and Fig. 2. All columns were H-150×150×22×22 mm build up section (H-overall depth (d_c)×flange width (b_f)×web thickness (t_w)×flange thickness (t_f)), The beams located on the first and second stories were H-150×100×12×20 mm.

The beams from the top story used a profile of double H-150x100x12x20 mm. All beams and columns satisfied the requirements for the seismic compact section according to AISC (2005) seismic provisions. The stiffness of the columns was sufficient to enable the development of the yield strength of the infill panel

$$I_c = 0.00307 \frac{w h_s^4}{L} \tag{1}$$

where I_c is the moment of inertia of the column; w is the infill panel thickness; h_s is the height of

Table 1 Sections and material properties of the specimens (Choi and Park 2008)

Specimen	Column Section, (σ_y)[a]	Beam Section, (σ_y)[a]	Brace Section, (σ_y)[a]	Plate Thickness, (σ_y)[a]
MRF	H-150×150×22×22 (348 MPa)	H-150×100×12×20 (377 MPa)	-	-
CBF	H-150×150×22×22 (348 MPa)	H-150×100×12×20 (377 MPa)	H-100×100×10×10 (393 MPa)	-
SPSW	H-150×150×22×22 (348 MPa)	H-150×100×12×20 (377 MPa)	-	4 mm (299 MPa)

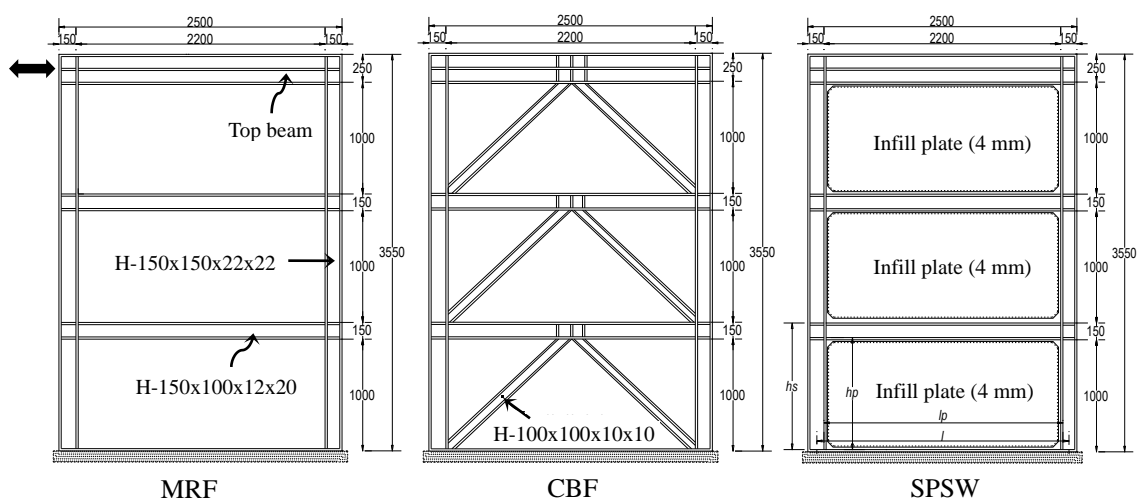[a]: Yield strenght of steel

Fig. 1 The configuration of the specimens (mm) (Choi and Park 2008)

Table 2 Sections and material properties of the structural members

Specimen	Column Section, $(\sigma_y)^a$	Beam Section, $(\sigma_y)^a$	SWR Diameter, $(\sigma_y)^a$
SWR36	H-150×150×22×22 (348 MPa)	H-150×100×12×20 (377 MPa)	36 mm (500 MPa)
SWR22	H-150×150×22×22 (348 MPa)	H-150×100×12×20 (377 MPa)	22 mm (500 MPa)

the column; and *L* is the width of the bay. The stiffness of the beams satisfied the requirements recommended in the SPSW design guide (AISC 2007)

$$I_b = 0.003 \frac{\Delta t_w L^4}{h_s} \tag{2}$$

where I_b is the moment of inertia for the beam; and Δt_w is the difference in the infill panel thickness bounding the horizontal member. The thickness of the infill plates in the SPSW model is 4 mm and with an aspect ratio (l_p/h_p) of 2.2. According to an elastic strain energy formulation (Thorburn 1983) the area of the brace members, *A*, in CBF is suitably comparable with that of SPSW

$$A = \frac{wL \sin^2 2\alpha}{2 \sin \theta \sin 2\theta} \tag{3}$$

where θ is the angle between the vertical axis and the equivalent brace and α is the angle of inclination of the principal tensile stresses in the infill plate measured vertically, which is given as (Thorburn 1983)

$$\tan^4 \alpha = \frac{1 + \frac{wL}{2A_c}}{1 + wh_s \left(\frac{1}{A_b} + \frac{h_s^3}{360 I_c L} \right)} \tag{4}$$

where A_c is the cross sectional area of the bounding column; I_c is the moment of inertia of the bounding column; h_s is the story height; A_b is the beam cross sectional area. The number and diameters of the steel wire ropes in SWR36 and SWR22 were calculated using the following equation, which was in turn derived from Eq. (3)

$$n = \frac{2wL \sin^2 2\alpha}{\pi R^2 \sin \theta \sin 2\theta} \tag{5}$$

where *n* and *R* is the number and diameter of steel wire rope, respectively.

2.2 Finite element modeling

Three-dimensional nonlinear finite element analyses were performed using ANSYS (2014) software. Material properties were defined by element type, material model and key options. Columns, beams and braces were modeled with eight node solid brick elements, SOLID185, showing stress stiffening, large deflection and large strain capabilities. Moreover, each node has three degrees of freedom as well as transition in the nodal x, y and z directions. Steel plates were modeled with SHELL181. SWRs were modeled with LINK180 and tension-only behavior was taken into consideration. Geometric and material nonlinearities were included in the solutions. To
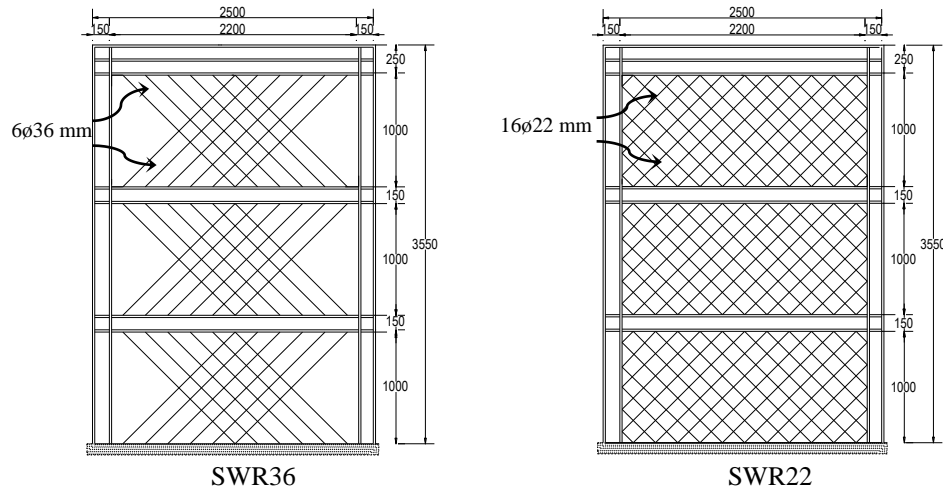
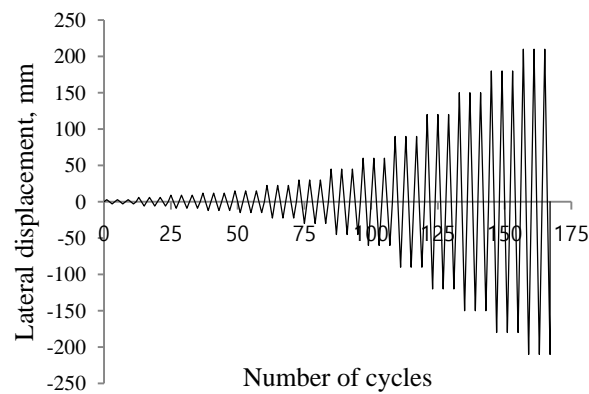Fig. 2 The configuration of the proposed SWR models (mm)

Fig. 3 Cyclic loading protocol

model metal plasticity behavior that occurs under cyclic loading, the bilinear kinematic hardening model, BKIN, including the Bauschinger effect, was used.

A quasi-static analysis was performed for each of the models and a complete undertaking of the Newton-Raphson method was used for nonlinear analysis. For displacement controlled cyclic loading, a total of 168 load steps (LS) were defined. All load steps were further divided into multiple substeps, until the total load was achieved. The same loading protocol, used by Choi and Park (2008), was also taken into consideration (Fig. 3),

3. Results and discussions

3.1 Verification of numerical results

Numerical results were verified by comparing hysteresis curves of MRF, CBF and SPSW with

Table 3 Results summary

		Maximum load						Maximum displacement					
		Positive loading (+)			Negative loading (-)			Positive loading (+)			Negative loading (-)		
	Specimen	P_{max} (kN)	δ (mm)	Story drift[a] (%)	P_{max} (kN)	δ (mm)	Story drift[a] (%)	P (kN)	δ_{max} (mm)	Story drift[a] (%)	P (kN)	δ_{max} (mm)	Story drift[a] (%)
Choi and Park 2008	MRF	453	150.7	4.5	-483	-149.1	4.4	391	211.4	6.3	-450	-241.5	7.2
	CBF	1419	22.8	0.7	-1421	-19.2	0.6	1125	60.7	1.8	-1115	-60.8	1.8
	SPSW	1798	150.9	4.5	-1817	-150.8	4.5	1776	181.3	5.4	-1776	-181.5	5.4
Numerical Study	MRF	438	150.0	4.3	-438	-150	4.3	432	210	5.9	-431	210	5.9
	CBF	1669	22.5	0.6	-1656	-22.5	0.6	1358	45	1.3	-1372	-45	1.3
	SPSW	1855	180	5.1	-1855	-180	5.1	1855	180	5.1	-1855	-180	5.1
	SWR36	934	45	1.3	-915	-45	1.3	799	150	4.3	-781	-150	4.3
	SWR22	1416	30	0.85	-1354	-30	0.85	1140	120	3.4	-1149	-90	2.5

		Yield point											
		Positive loading (+)						Negative loading (-)					
	Specimen	P_y (kN)	δ_y (mm)	Story drift[a] (%)	K_y^{b} (kN/mm)	P_{max}/P_y	μ_y^{c}	P_y (kN)	δ_y (mm)	Story drift[a] (%)	K_y^{b} (kN/mm)	P_{max}/P_y	μ_y^{c}
Choi and Park 2008	MRF	419	59.0	1.75	7	1.08	3.58	-430	-47.5	1.41	9	1.12	5.08
	CBF	1272	14.3	0.42	89	1.12	4.24	-1256	-13.5	0.40	93	1.13	4.50
	SPSW	1653	15.5	0.46	107	1.09	11.70	-1651	-15.4	0.46	107	1.10	11.78
Numerical Study	MRF	356	45	1.26	7.91	1.23	4.67	-356	-45	1.26	7.91	1.23	4.67
	CBF	1509	15.6	0.44	97	1.11	2.88	-1464	-15	0.42	97.6	1.13	3
	SPSW	1601	12	0.3	133	1.16	15	1602	-12	0.3	133	1.16	15
	SWR36	720	15	0.42	48	1.3	10	-707	-15	0.42	47.1	1.3	10
	SWR22	1288	22.5	0.64	57.2	1.1	5.33	-1249	-22.5	0.64	55.5	1.09	4

[a]: Maximum displacement at top divided by wall height, [b]:Initial stiffness; $K_y = P_y / \delta_y$,
[c]: Displacement Ductility; $\mu_y = \delta_{max} / \delta_y$

experimental results being represented by the study of Choi and Park (2008), Results at yield point, maximum load and maximum displacement of specimens are summarized in Table 3. The maximum displacement (δ_{max}) of the CBF and SWR22 specimens showing softening behavior was defined as the value corresponding to 0.8 times the maximum load. Hysteresis curves of top lateral displacements versus base shear force of MRF, CBF and SPSW specimens are given in Fig. 4 and Fig. 5, respectively.

In the analysis of MRF, during the 3rd cyclic loading of 45 mm displacements (LS-53), plastic hinges developed at the ends of the beams (Fig. 6(a)). After this point, the load-displacement curve became horizontal. In the numerical study, 438 kN maximum load was obtained at 150 mm displacement, whereas in the experimental study (Choi and Park 2008) the maximum load was 453 kN with 150.7 mm displacement. In the following cycles, plastic hinges developed in the bases of the columns. In the 210 mm displacement, net sectional yielding occurred in the columns bases and beam endings which affected the load bearing capacity (Fig. 6(b)), Initial stiffness was
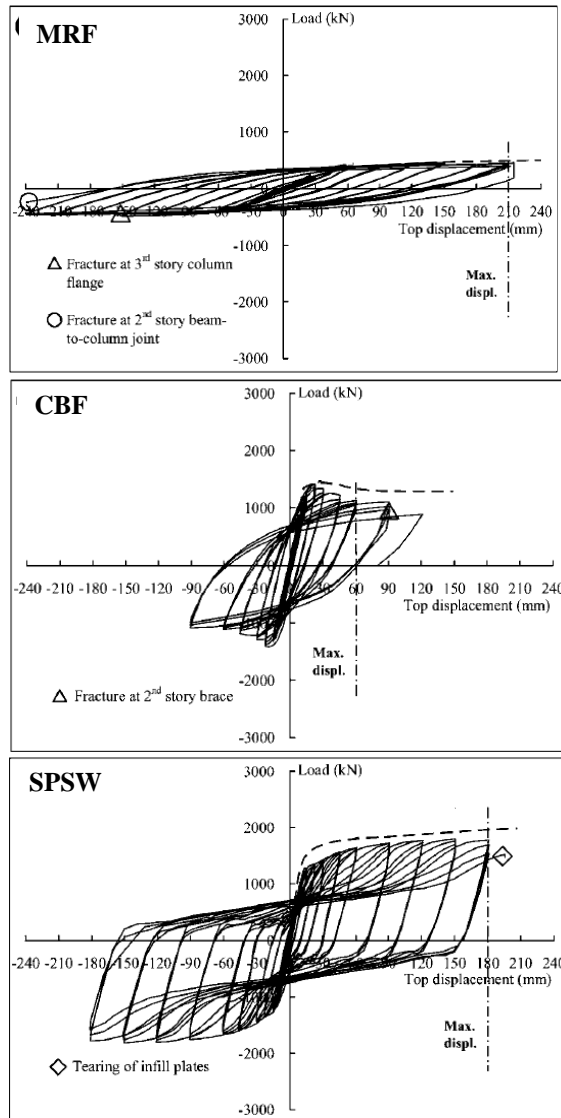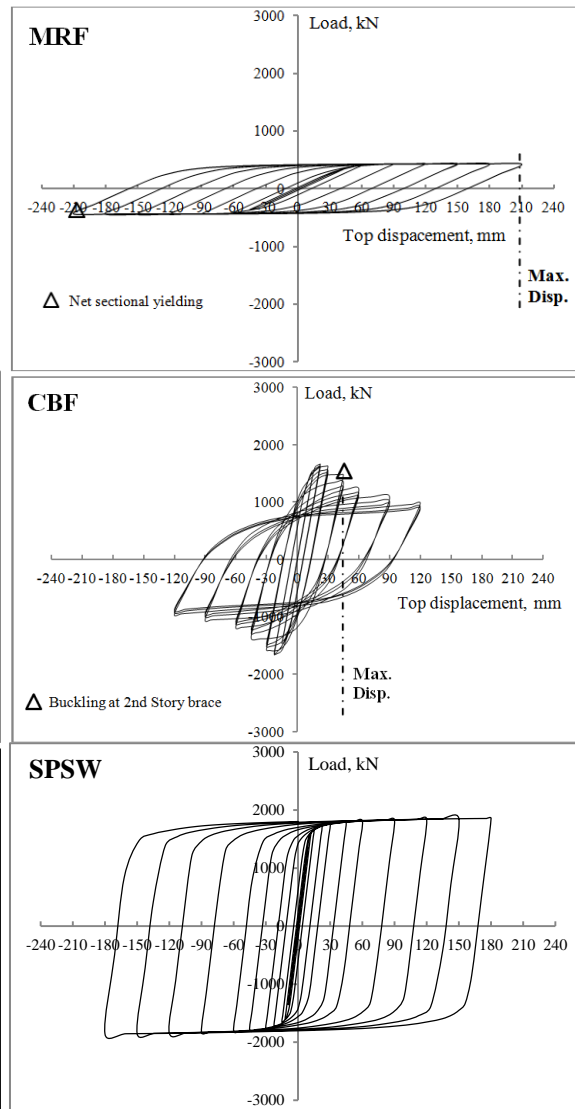
Fig. 4 Experimental results


Fig. 5 Numerical results

obtained at 7.91 kN/mm whereas in the experimental study it was 7 kN/mm (Table 3).

The CBF specimen showed gradually decreasing load carrying capacity after the maximum load (Figs. 4 and 5), In the analysis of CBF, for both experimental and numerical studies, buckling took place in the midspan of compression braces with a 30 mm displacement (LS-73) (Fig. 7). In the experimental study 1419 kN maximum load was obtained with a 22.8 mm displacement. In the numerical study, maximum load was 1669 kN with a 22.5 mm displacement.

Initial stiffness was 89 kN/mm in the experimental study, while measuring 97 kN/mm in the numerical study. At the LS-93 (δ=45 mm) in the midspan of the 2nd story braces, fractures were observed (Fig. 8). Until this point, no plastic strain was observed in the columns. Buckling that took place on the 2nd story resulted in additional shear force on that story which in turn led to
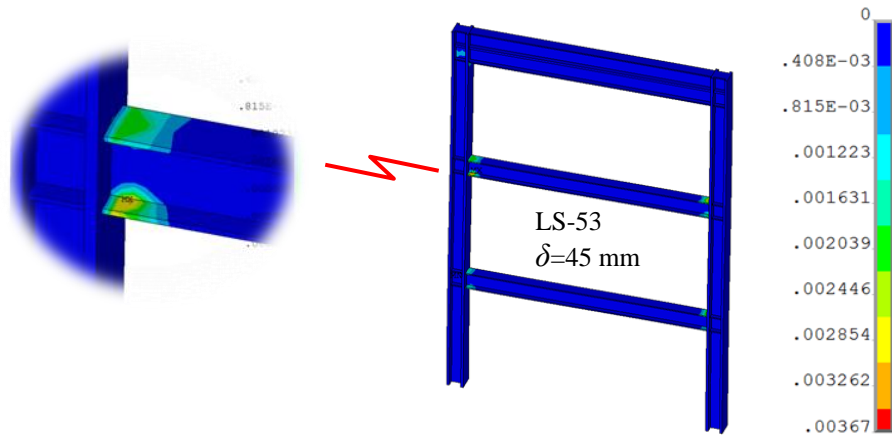
(a)
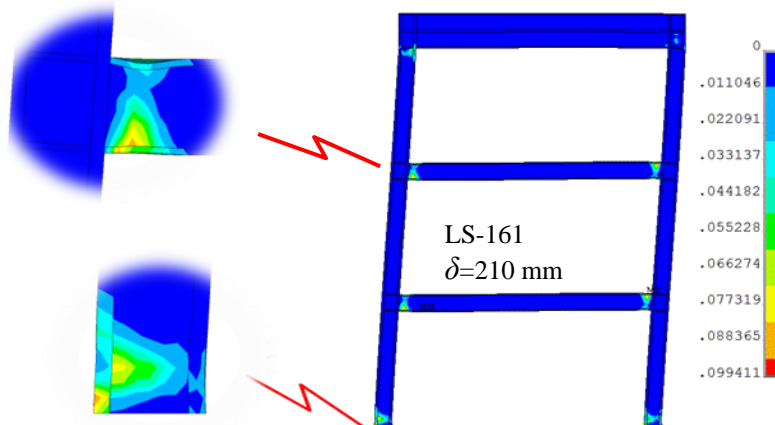
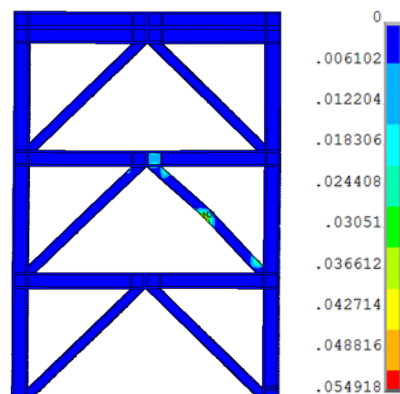(b)

Fig. 6 Plastic strains in MRF; (a) first yielding; (b) end of test
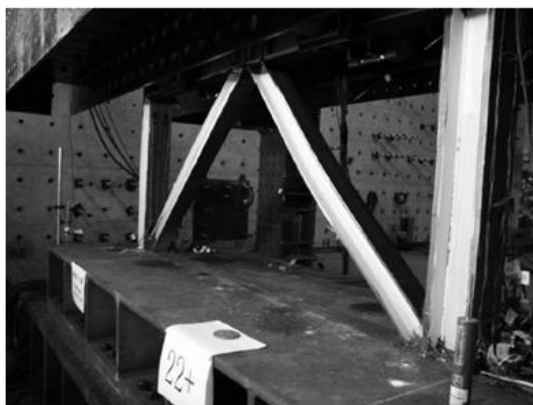
(a)   (b)

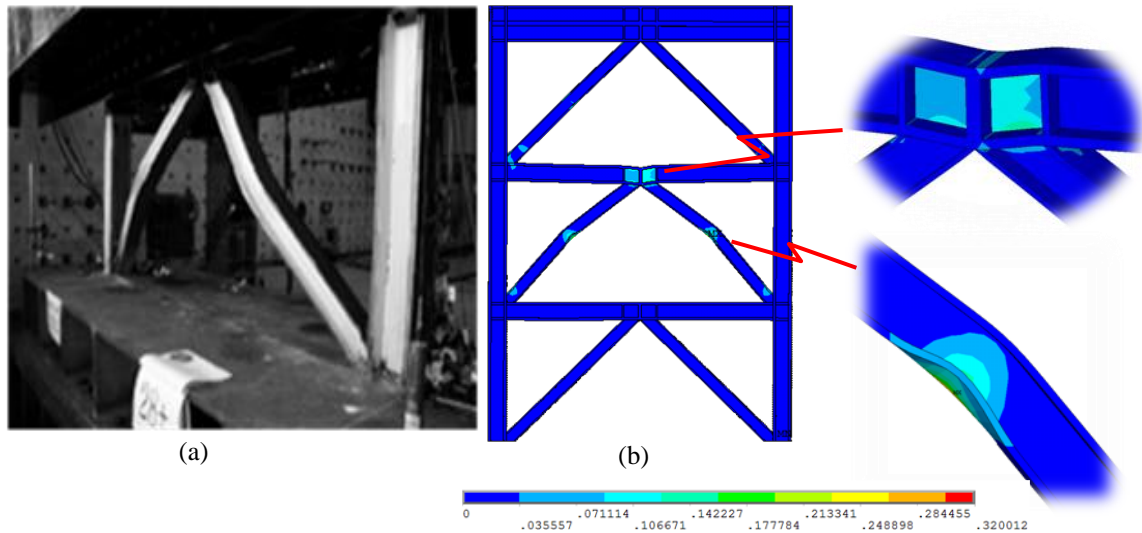Fig. 7 Buckling of 2nd story compression brace, δ= 30 mm; (a) experimental; (b) numerical

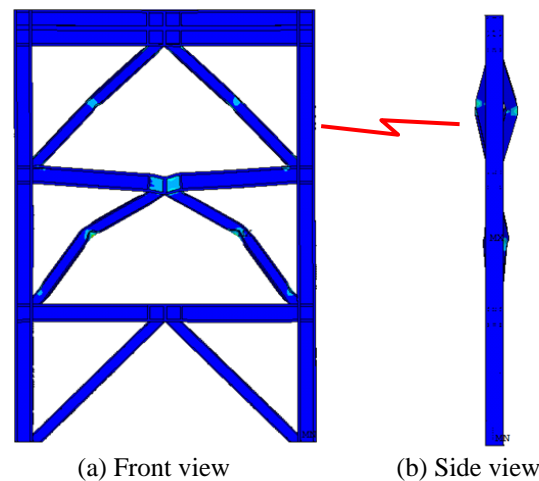Fig. 8 Net sectional yielding at the center of compression braces, δ= 45 mm (a) experimental; (b) numerical

(a) Front view   (b) Side view

Fig. 9 Out of plane buckling on 3rd story braces at the end of analysis

extreme plastic strains within the second story beam (Fig. 8). Because of this additional vertical load caused by buckling of the brace, 2nd story beam deflected downward. After this cycle, the development of plastic hinges increased exponentially on this story. As a result, stiffness and strength at the 2nd story were significantly reduced. In the developing cycles, load carrying capacity decreased as the plastic deformation increased and out of plane buckling were seen on the 3rd story braces (Fig. 9). In the experimental study, buckling occurred in the 1st and 2nd stories while in this numerical study buckling occurred in the 2nd and 3rd stories (Fig. 9).

SPSW specimen showed stable ductile behavior. In the numerical study, the first yielding happened at the level of 1601 kN loading with 12mm displacement in the infill plate-beam boundary zone. There is a difference when compared to the experimental study which showed a
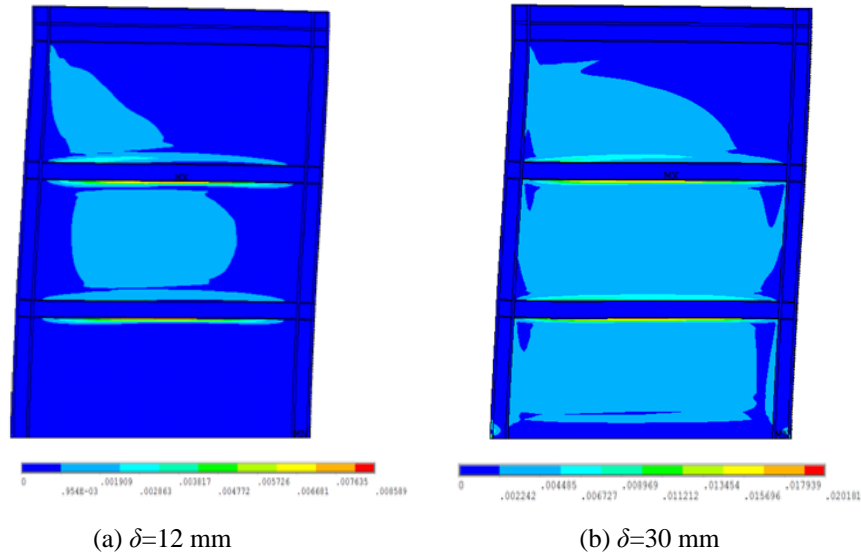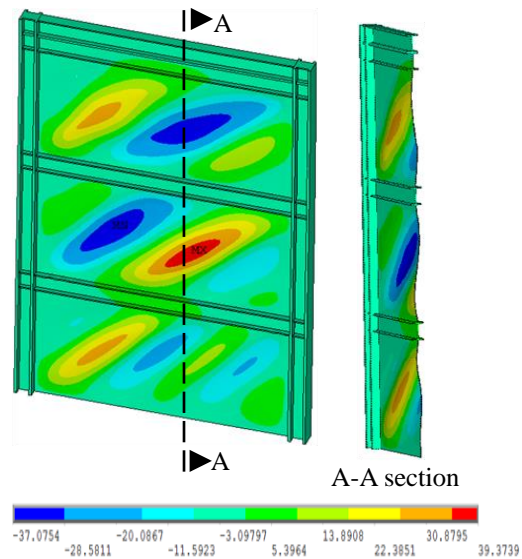
(a) δ=12 mm   (b) δ=30 mm

Fig. 10 Plastic strain developments and tearing of infill plates in SPSW

A-A section

Fig. 11 Out of plane buckling at δ=30 mm

level of 1653 kN loading with a 15.5 mm displacement (Fig. 10(a)). At the 30 mm displacement local out of buckling and tension field action of infill plates developed in all stories (Figs. 10(b) and 11). After all infill plates yielded, plastic hinges developed at the ends of beams and at the column bases by the moment frame action (Fig. 12). At 180 mm displacement, yield zone was concentrated at the column bases and the system lost its load bearing capacity (Fig. 12). In the numerical study, maximum load was obtained with 1855 kN with 180 mm displacement, however, in the experimental study, it was 1798 kN with 150.9 mm displacement.
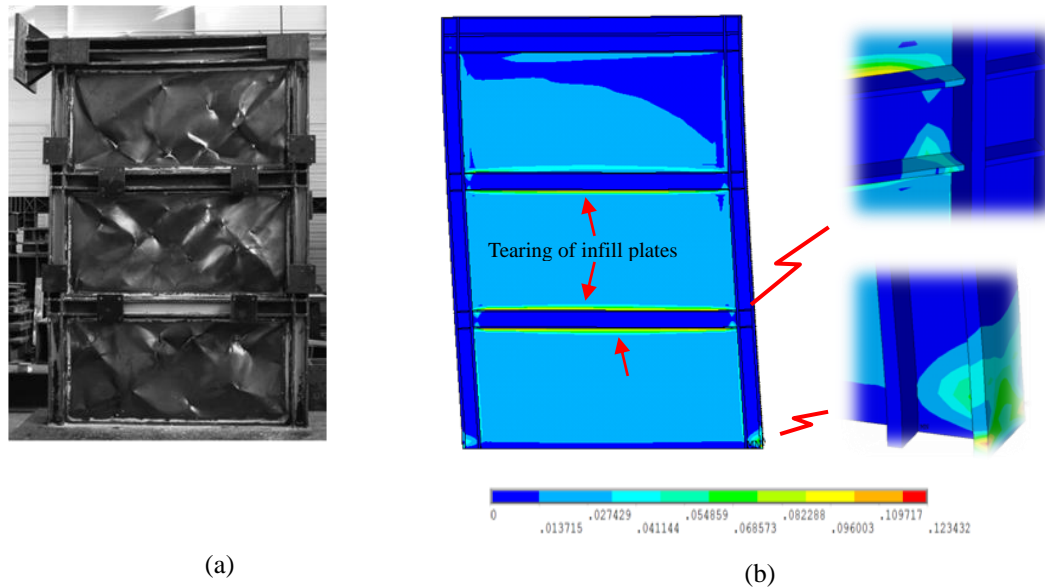
(a)   (b)

Fig. 12 Deformed shapes of SPSW at the end of the analysis; (a) experimental; (b) numerical
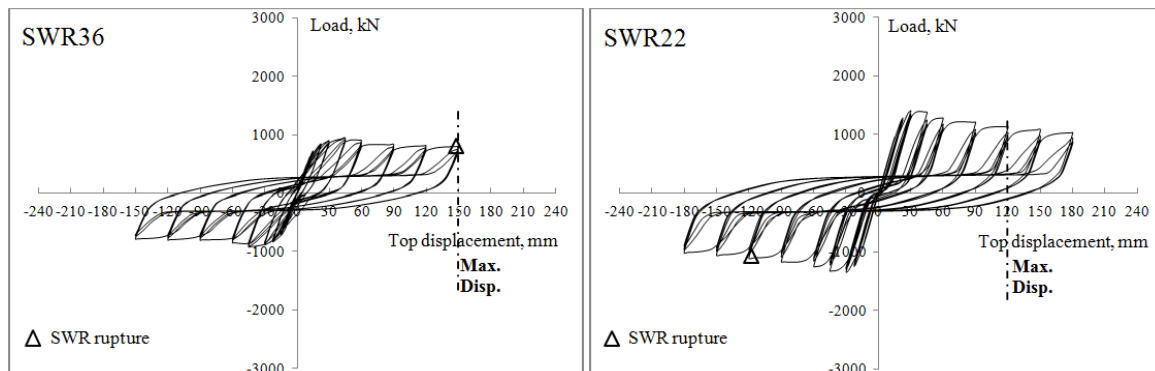

Fig. 13 Load-displacement relationships of SWR specimens

3.2 Effect of SWRs

Numerical results show a good level of agreement with experimental results, though it overestimated the reverse cycles of SPSW. The finite element analysis adequately predicted the load carrying capacities of the MRF, CBF and SPSW specimens as well as the corresponding lateral displacements. In this section, the effects of SWRs are discussed and compared with the numerical results of MRF, CBF and SPSW specimens. Hysteresis curves of top lateral displacements versus base shear force of SWR22 and SWR36 specimens are given in Fig. 13. The envelope curves of the load-top displacement of the specimens are shown in Fig. 14.

In the SWR36, the first yielding happened with 15 mm displacement at the SWR-beam boundary zone. (LS-49) In that moment, 720 kN load obtained with 45 kN/mm initial stiffness. Furthermore, maximum load was obtained at the 934 kN loading level at 45 mm displacement.
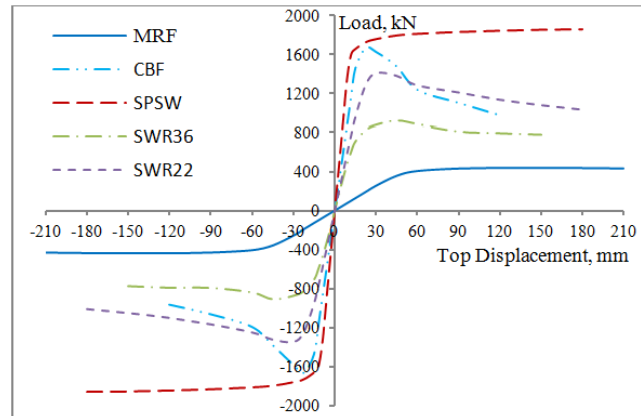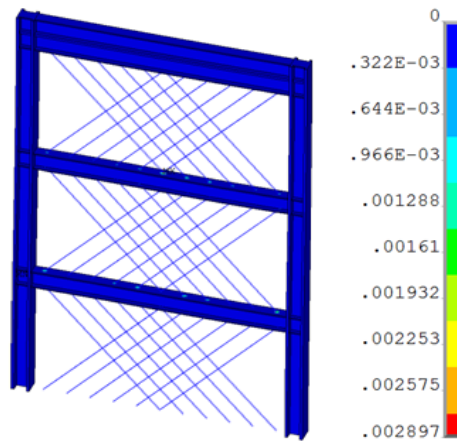
Fig. 14 Envelope curves of specimens

Fig. 15 Von Mises plastic strain at δ= 45 mm

After this point, deformations in the SWR-beam boundary zone on the 2nd and 3rd stories increased, along with plastic hinges occurring at the ends of the beams, however, no plastic strains were observed on the columns (Fig. 15). In the developed cycles, in the SWR-beam boundary zone of the 2nd story, failures were observed and maximum displacement was obtained in the 3rd cycle at 150mm displacement (LS-141) (Fig. 16). SWR36 carried a maximum load at 106% more than MRF (Table 3, Fig. 14). Moreover, the initial stiffness of SWR36 was 570% more than MRF, 50% less than CBF and 66% less than SPSW.

In the SWR22 specimen, first yielding occurred at the SWR-beam boundary zones in 22.5mm displacement (LS-65), At that level 1288 kN load was obtained while initial stiffness was calculated at 57.2 kN/mm. Maximum load was obtained at 1416 kN with 30 mm displacement. After this point, plastic strains increased at the SWR-beam boundary zones of the 2nd story but no significant damage happened within the SWR-column boundary zones (Fig. 17). In the developed cycles, on the SWR-beam boundary zones of the 2nd story, some failures happened at 120 mm maximum displacement (LS-121) (Fig. 18). The SWR22 specimen carried a load 223% more than MRF, 15% less than CBF and 23% less than SPSW. Moreover the initial stiffness of the SWR22
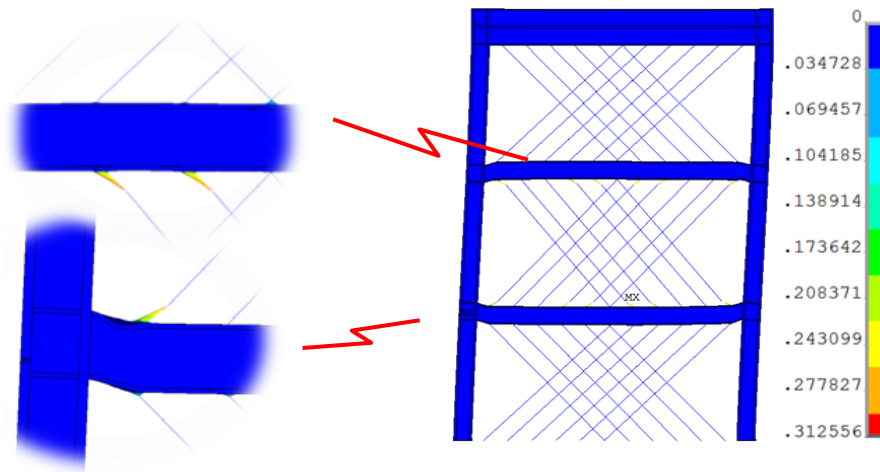
Fig. 16 Failure at SWR-beam boundary zones, and plastic hinge formation at the ends of the beams
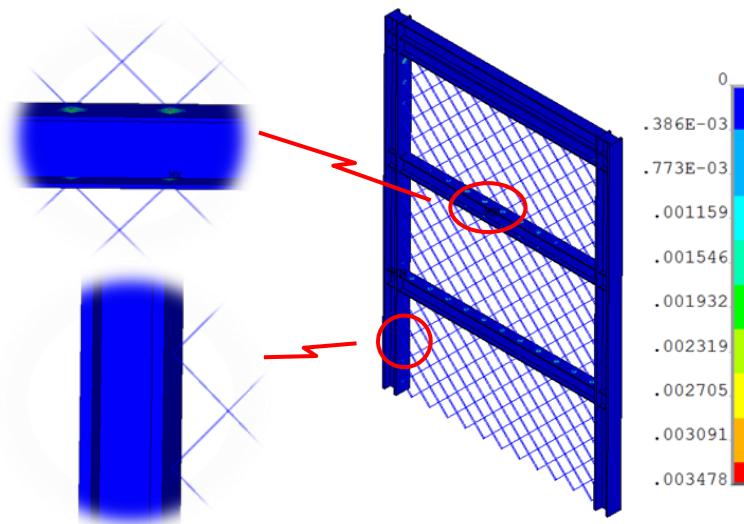

Fig. 17 Von Mises plastic strain at δ= 22.5 mm

specimen was 623% more than MRF, 41% less than CBF and 57% less than SPSW. Both SWR36 and SWR22 showed stable load-displacement behavior without any sudden decrease in strength.

3.3 Deformation capacity and ductility

Among numerical results, CBF showed considerably low deformation capacity (1.3% drift) because of early buckling of compression braces. MRF exhibited large deformation capacity (5.9%), SPSW exhibited ductile behavior as yielding of infill plates distributed along the high of the wall at all stories. As a result, SPSW showed, with a drift of 5.1%, the closest deformation capacity to MRF. However, MRFs' initial stiffness and strength were relatively low. SPSW,
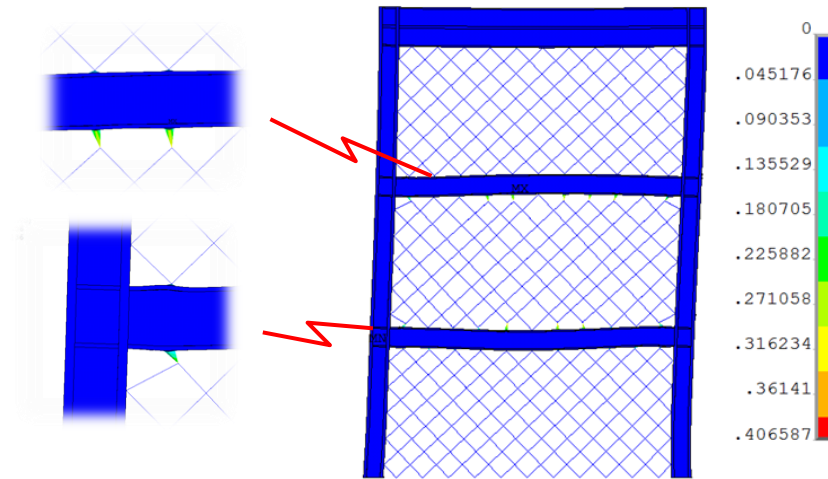
Fig. 18 Damage situation of SWR22 at *δ*=120 mm

SWR36 and SWR22 showed shear dominated behavior. In SWR36 and SWR22, plastic deformations were uniformly distributed to all wire ropes and boundary zones. SWR36 and SWR22 specimens reached 4.3% and 3.4% drift ratios, respectively. These results indicated that the deformation mode determined the deformation capacity and ductility. However, when it comes to the goals of design meant to withstand earthquakes to the greatest degree possible, the ductility capacity that represents the combined capacity of deformation and initial stiffness is more important than the deformation capacity. The ductility ratios of the specimens were calculated by using the ratio of lateral displacement measured at yielding load to the measured at the point where the ultimate load capacity decreased to 80%. The ductility ratio of the SPSW specimen reached 15, while the MRF specimen reached 4.67. Additionally, SPSW behaved more rigidly than MRF with its 133 kN/mm initial stiffness (Table 3, Fig. 19), CBF had a displacement ratio of 3 and initial stiffness of 97 kN/mm. SWR36 and SWR22 had displacement ratio of 10 and 4, respectively and showed better behavior than CBF. However, their initial stiffness less than CBF with the ratio of 50% and 41%, respectively.

For each specimen, stiffness degradation were calculated for each cycle (Fig. 19). Stiffness degradation were started at 0.43% lateral drift for SWR22 and CBF while it was 0.20% for SPSW. However, CBFs stiffness degradated rapidly among the other specimens. This result indicated that the local buckling of the braces was the primary cause of the stiffness degradation. Stiffness degradation characteristic of SWR22 and SWR36 specimens showed similar behavior to SPSW, because, plastic deformations were uniformly distributed to all stories.

The area under the hysteresis loops is a measure of the energy dissipated through nonlinear hysteretic behavior. For each specimen, energy dissipation was determined by calculating the areas inside the hysteretic load–displacement loops for each cycle. The cumulative energy dissipation was defined as the sum of the areas enclosed by all previous hysteresis loops. Energy dissipation values were plotted against the corresponding lateral drift values. Fig. 20 shows the variation of cumulative energy dissipation characteristics of the specimens. The energy dissipation capacity of SPSW was greater than the other specimens whereas MRF dissipated less energy. SWR22 dissipated more energy than CBF and SWR36 with more deformation capacity. The energy
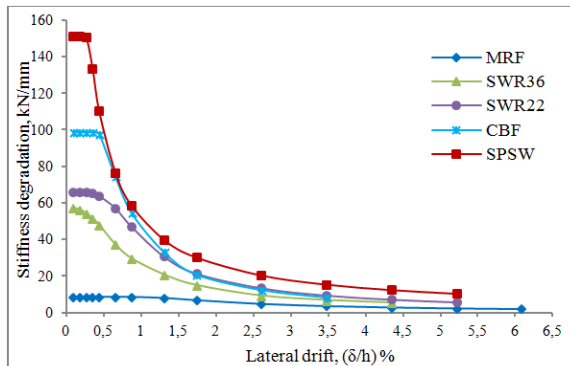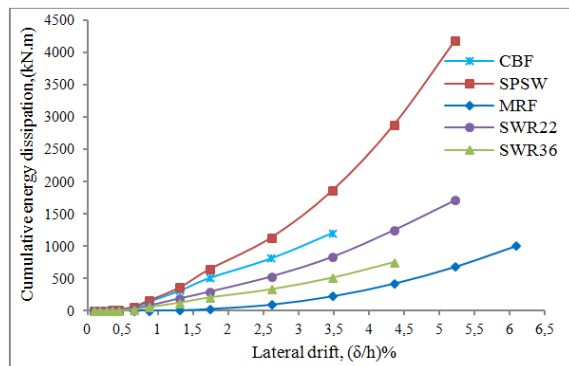
Fig. 19 Stiffness degradations

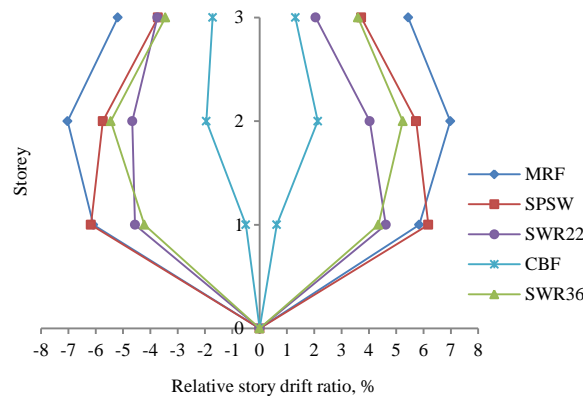Fig. 20 Cumulative energy dissipation capacities

Fig. 21 Variations of maximum relative story drifts

dissipation capacity of SWR specimens increased with the number of steel wire ropes. SWR22 dissipated more energy than SWR36 by tension field action on columns. At the drift of 4.3%, the ratios of the energy dissipation capacities of SWR36 and SWR22 to that of MRF were 1.79 and 2.98, respectively. The energy dissipation capacity of CBF was similar to that of SPSW, before the buckling of the brace (0.87% drift),

Fig. 21 shows variation of relative story drift of specimens. In all specimens except CBF, the drift at the first story was greater than upper stories. Due to the detrimental soft-story failure mechanism, in CBF, maximum story drift occurred in 2nd story. Both SWR22, SWR36 and SPSW show relatively uniform story drift along the stories.

4. Conclusions

In this study, the behavior of steel frames which is strengthened with diagonally braced multi-cables were examined. For this purpose, five different three dimensional numerical models were analyzed. Numerical results obtained from cyclic loadings were compared with the experimental studies of Choi and Park (2008). The findings obtained in the present study are summarized as follows:

• SWR specimens showed stable ductile behavior without any sudden decrease in strength.

• The local fracture of cables did not significantly affect the overall strength and deformation capacity of the system. It is the most important advantage of multi-cable usage.

• Moment resisting frames strengthened with multi-cables showed better initial stiffness and strength according to bare frames. This retrofitting method can increase the lateral stiffness without reducing the moment frame ductility.

• The energy dissipation capacity of SWR specimens increased with the number of cables.

• The energy dissipation capacity of SWR22 increased by the tension field action developed by the cables. Therefore to improve the tension field action, it is suggested that cables should be restrained between beams and columns instead of beams to beams.

• Failure in the SWR specimens occurred in the boundary zones of the cables and beams. That is why boundary zone must have enough stiffness and strength to resist tension field action of SWRs, otherwise a soft story can be developed.

• In the CBF, as a result of early buckling of compression brace, the stiffness and strength significantly reduced and soft story failure mechanism observed likewise earlier studies in the literature.

• The multi-cable system can be used for the rapid strengthening of low-rise industrial, commercial and residential steel buildings because of its relative ease to produce and finance.

References

Aguero, A., Izvernari, C. and Tremblay, R. (2006), "Modelling of the seismic response of concentrically braced steel frames using the OpenSees analysis environment", *Int. J. Adv. Steel Constr.*, **2**(3), 242-274.

American Institute of Steel Construction (AISC) (2005), Specification for Structural Steel Buildings, Chicago.

American Institute o f Steel Construction (AISC) (2007), Steel Plate Shear Walls, Chicago.

Ansys Mechanical (2014), Ansys Inc., Canonsburg, PA.

Broderick, B.M., Elghazouli, A.Y. and Goggins, J. (2008), "Earthquake testing and response analysis of concentrically-braced sub-frames", *J. Constr. Steel Res.*, **64**, 997-1007.

Choi, I.R. and Park, H.G. (2008), "Ductility and energy dissipation capacity of shear dominated steel plate walls", *J. Struct. Eng.*, **135**(7), 785-796.

Fanaie, N., Aghajani, S. and Dzaj, E.A. (2016), "Thearetical assessment of the behavior of cable bracing system with central steel cylinder", *Adv. Struct. Eng.*, **19**(3), 463-472.

Filiatrault, A. and Tremblay R. (1998), "Design of tension-only concentrically braced steel frames for seismic induced impact loading", *Eng. Struct.*, **20**(12), 1087-1096.

Gupta, A. and Krawinkler, H. (1999), "Seismic demands for performance evaluation steel moment resisting frame structures", Report No. 132, The John A. Blume Earthquake Engineering Center, Dept. of Civil and Env. Eng., Stanford University.

Hadi, M.N.N. and Alrudaini, T.M.S. (2012), "New building scheme to resist progressive collapse", *J. Arch. Eng.*, **18**(4), 324-331.

Hou, X. and Tagawa, H. (2009), "Displacement-restraint bracing for seismic retrofit of steel moment frames", *J. Constr. Steel Res.*, **65**(5), 1096-1104.

Mousavi, S.A., Zahrai, S.M. and Saatcioglu, M. (2015), "Toward buckling free tension-only braces using slack free connections", *J. Constr. Steel Res.*, **115**, 329-345.

Mousavi, S.A. and Zahrai, S.M. (2016), "Contribution of pre-slacked cable braces to dynamic stability of non-ductile frames; an analytical study", *Eng. Struct.*, **117**, 305-320.

Sabelli, R. and Bruneau, M. (2007), "Steel Plate Shear Walls (AISC Design Guide)", American Institute of

Steel Construction, Inc., Chicago, Illinois.

Tamai, H. and Takamatsu, T. (2005), "Cyclic loading test on a non-compression brace considering performance based seismic design", *J. Constr. Steel Res.*, **61**(9), 1301-1317.

Thorburn, L.J., Kulak, G.L. and Montgomery, C.J. (1983), "Analysis of steel plate shear walls", Structural Engineering Rep. No. 114, Dept. of Civil Engineering, Univ. of Alberta, Edmonton, Albta., Canada.

Timler, P.A., Ventura, C.E., Prion, H. and Anjam, R. (1998), "Experimental and analytical studies of steel plate shear walls as applied to the design of tall buildings", *Struct. Des. Tall Build.*, **7**, 233-249.

Tremblay, R. and Filiatrault, A. (1996), "Seismic impact loading in inelastic tension-only concentrically braced steel frames: myth or reality?", *Earthq. Eng. Struct. Dyn.*, **25**, 1373-1389.

Tremblay, R. (2001), "Seismic behavior and design of concentrically braced frames", *Eng. J.*, **38**(3), 148-66.

Wang, W., Zhou, Q., Chen, Y., Tong, L. and Chan, T.M. (2013), "Experimental and numerical investigation on full-scale tension-only concentrically braced steel beam-through frames", *J. Constr. Steel Res.*, **80**, 369-385.

CC